JMEPEG (2011) 20:1583–1590
DOI: 10.1007/s11665-010-9812-0

1059-9495/$19.00

Effect of Process Parameters on Microstructure and Micro-hardness of AZ91/Al_2O_3 Surface Composite Produced by FSP

Ghader Faraji, Omid Dastani, and S. Ali Asghar Akbari Mousavi

(Submitted August 19, 2010; in revised form November 29, 2010)

In this article, the effects of three different sizes of Al_2O_3 particles in the friction stir processing on grain size, cluster size, microstructure, and micro-hardness of as-cast magnesium alloy AZ91 were investigated. Moreover, the effects of two types of tool geometries and number of passes on the mentioned parameters were considered. Effect of mentioned parameters on microstructure, grain refinement, and micro-hardness profile in the friction stirred zone of the specimens was compared by as-cast received form and also friction stir processed (FSPed) specimens without particles. Microstructural characterization of the materials revealed reasonably uniform distribution of Al_2O_3 reinforcement and significant grain refinement. Hardness studies revealed that the incorporation of nano- and micro-size Al_2O_3 particulates in magnesium matrix led to a simultaneous increase in hardness.

Keywords AZ91, FSP, micro-hardness, microstructure, surface treatments

1. Introduction

The ability of magnesium (Mg)-based materials to exhibit high specific mechanical properties and to offer significant weight savings has fueled significantly research activities in recent times targeted primarily for their further development (Ref 1). Applications stretch from aerospace and automobile industries in replacement of aluminum and steel to electronic and computer industries in replacement of plastics (Ref 1). However, the mechanical properties, such as the hardness of the magnesium alloys, are not sufficient to enhance their applications. Though some processes to fabricate ceramics particle/magnesium alloys composites have been studied to improve the mechanical properties (Ref 1-11). Much attention has been paid to increase the mechanical properties of AZ31 magnesium alloy by friction stir processing (FSP), which is a similar process as friction stir welding (FSW) (Ref 2-6). Meanwhile, because of difficulties in FSP of AZ91Mg alloy and lack of AZ91 sheet form, working on AZ91 composite manufacturing by FSP was limited. Therefore, researchers have used different casting methods for manufacturing of AZ91/ceramic particles composite (Ref 1, 7-10).

For most isotropic composites, the micro-sized whiskers or particulates with a reinforcement volume fraction of 15-35% are commonly added into metallic alloys. In terms of grain size refinement and particle strengthening, one of the critical microstructure parameters is the particle interspacing L, which can be roughly estimated from $L = (d/2)(2\pi/3Vf)^{1/2}$ (Ref 12) where d is the average particle diameter and Vf is the particle volume fraction. With reinforcing particles of $Vf = 20\%$ and $d = 20$ μm in typical aluminum-based composites, L will be about 32 μm. According to the above equation, as the reinforcement size d decreases to the 10-50 nm range, the composites only need a small volume percentage of reinforcing particles to result in the interspacing being in the 100-1000 nm range (Ref 13).

In this study, Al_2O_3 particles with three different sizes (ranging from nanometer to micrometer scale) were dispersed into AZ91 as-cast in order to reveal the effect of the FSP with the Al_2O_3 particles on the microstructure and hardness of the magnesium alloy AZ91. Two square and triangular type tools were used in the process. Effect of FSP tool geometry on microstructure, grain refinement, and micro-hardness has been investigated. The process was carried out in single and three numbers of passes to reveal the number of passes effect on grain size, cluster size, and micro-hardness of the AZ91 as-cast and Al_2O_3 particulate surface composite.

2. Experimental Procedure

Commercially available Al_2O_3 powder with three different sizes (ranging from nanometer to micrometer scale) 3000, 300, and 30 nm, and 99.9% pure was used. The Al_2O_3 powder was filled into a groove 0.8 mm (width) × 2 mm (depth) machined on the as-cast AZ91 plate of 3-mm thickness before the FSP was carried out. The material used in this work was an AZ91 as-cast magnesium alloy with the following composition (wt.%) Al, 8.9; Zn, 0.79; Si, 0.0091; Cu, 0.0014; Ni, 0.0011; Fe, 0.0017; Be, 32 ppm; Mg, balance. Two square and

Ghader Faraji, School of Mechanical Engineering, University College of Engineering, University of Tehran, Tehran, Iran; and **Omid Dastani** and **S. Ali Asghar Akbari Mousavi**, School of Metallurgy and Materials Engineering, University College of Engineering, University of Tehran, Tehran, Iran. Contact e-mail: gfaraji@engmail.ut.ac.ir.

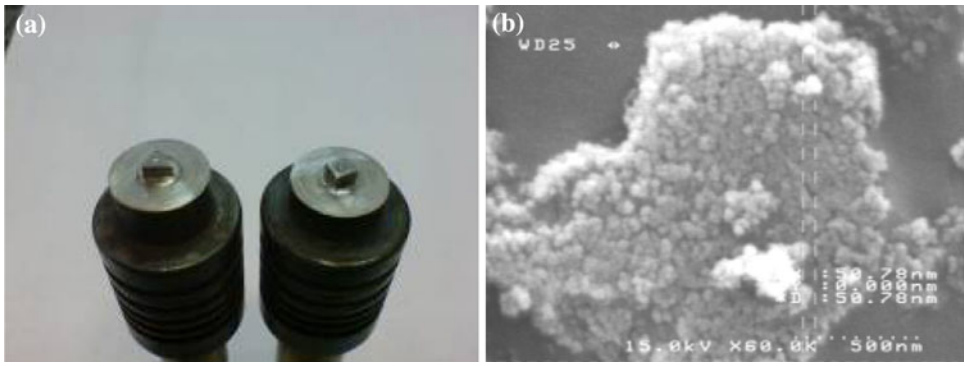

Fig. 1 (a) Picture of process tools (triangular, square) and (b) SEM micrograph of nano-particles

Table 1 Friction stir processing parameters investigated in this study

Specimen number	(1)	(2)	(3)	(4)	(5)	(6)
Particle size, μm	0.03	0.3	3	0.3	0.3	0.3
Tool type	Square	Square	Square	Triangular	Triangular	Square
Pass number	1	1	1	1	3	3

Fig. 2 Top face of the specimen produced by FSP

triangular FSP tools were used in this work; tools are made of hardened H13 tool steel and consist of a pin with 5-mm diameter, 1.8-mm height, and a 15-mm diameter shoulder (see Fig. 1).

The probe was inserted into the groove filled with the Al_2O_3 powder. A constant tool rotating rate of about 900 rpm was adopted and the constant travel speed was about 63 mm/min.

The welding tool was rotated in the clock-wise direction. The tilted angle was 3°. Transverse sections of the as-cast AZ91, as-produced friction stir processed (FSPed) samples with and without particles were cut for metallographic investigation. Surfaces were prepared by standard metallographic techniques and etched with a solution of 5 mL acetic acid, 6 g picric acid, 10 mL water, 100 mL ethanol, 5 mL HCl, and 7 mL nitric acid for 3-5 s.

The distribution of the Al_2O_3 particles, microstructure and material flow observation was carried out by optical microscopy of Olympus. The micro-hardness tests were performed on the samples prepared for microstructure observations by ESEWAY hardness tester. The Vickers micro-hardness tests (Hv) were conducted by using 200 g loads. At least five separate measurements were performed on each sample. X-ray diffraction (XRD) measurements were performed using a Scintag XDS2000 x-ray diffractometer. Cu Kα including $K\alpha_1 = 1.54056$ Å and $K\alpha_2 = 1.54439$ Å was used to collect data. XRD was used for investigation of changes in crystallographic lattice of AZ91 before and after FSP. To avoid misrepresentation of intensity, the XRD intensities were acquired in Debye-Scherrer geometry. The data were collected on a STOE diffractometer, Stadi P (Cu Kα radiation), equipped with a position sensitive detector (PSD, 0.03° angular resolution). The XRD scans were evaluated using DIFFRAKT 97, which allows profile fitting with high accuracy for each of the reflections separately. The local microstructure information was established by scanning electron microscopy (SEM) of CamScan MV2300. Table 1 shows the investigated process parameters. Alumina particle sizes used in this study were ~30 nm, 300 nm, and 3 μm. FSP tests were carried out in one and three passes. Figure 1(a) shows the picture of triangular and square FSP tools. SEM micrograph of alumina particles are shown in Fig. 1(b).

3. Results and Discussion

Figure 2 shows the surface appearances of surface nanocomposite layer produced by FSP. Defects such as voids and cracks are not observed on the surface. The top surface shows very smooth quality with particular rings and there are almost no prominences or depressions, in spite of the tool's stirring.

Figure 3 shows optical micrograph of the cross section of the FSPed specimen produced by triangular type tool, in which the rotational and traverse speed was 900 rpm and 63 mm/min, respectively. In this case, Al_2O_3 particle size was 300 nm. This figure shows that there are no defects and porosities in the cross section of the FSPed specimen.

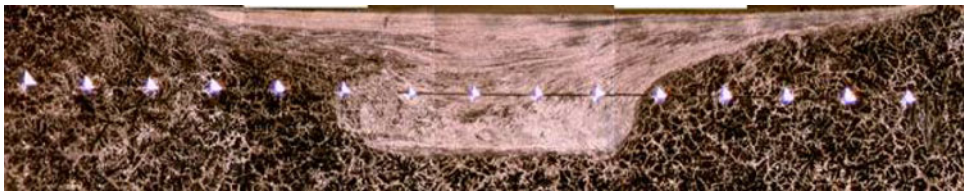

Fig. 3 Optical micrograph of cross-sectional FSPed specimen by triangular tool in single pass

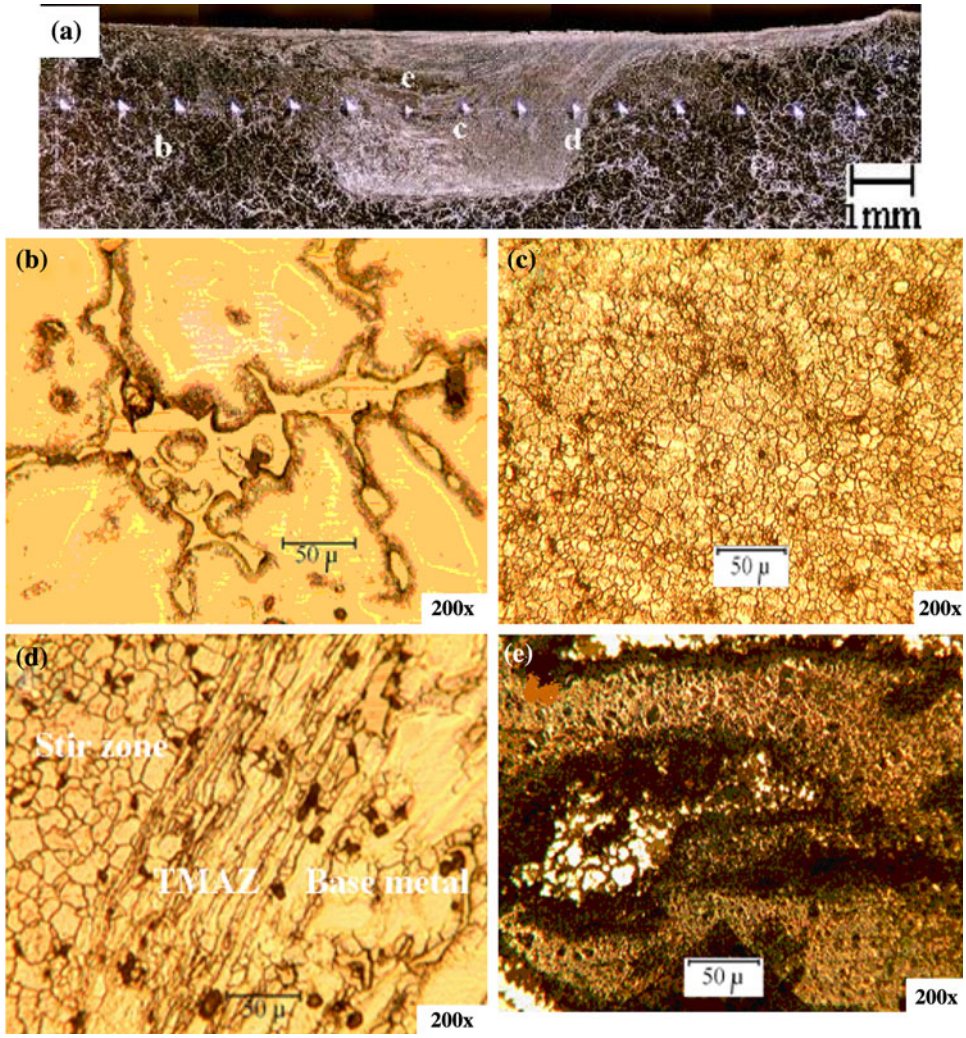

Fig. 4 (a) Macro-image of the cross section of FSPed specimen, (b) BM, (c) SZ, (d) stir zone, TMAZ (equiaxed grains) base metal, and (e) the particle agglomerated zone

3.1 Microstructure

Figure 4(a) shows the macro-image of the weld zone of FSPed specimen produced by square type tool, along with the optical microstructures of the base metal (BM, Fig. 4b), the stir zone (SZ, Fig. 4c), thermo-mechanical affected zone (TMAZ, Fig. 4d), and particle agglomerated zone (Fig. 4e). A representative microstructure of the BM is shown in Fig. 4(b), where the relatively dark colored β-phase ($Mg_{17}Al_{12}$) is embedded at the grain boundaries of the light colored α-phase. Figure 4(c-e) represents the TMAZ, SZ, and particle agglomerated zone, respectively. The transition region between the SZ and BM are observed in the TMAZ (Fig. 4d). The grains in the TMAZ are continuously aligned in a direction and finely some equiaxed grains are observed. One can see some grain refinement in this region. Region "c" is characterized by the presence of a recrystallized grain structure and homogeneously distributed particles. The recrystallized grains were equiaxed and have a similar size distribution. Al_2O_3 particles were found to be distributed within this region due to the occurrence of vigorous stirring during the process. Grain structures in the SZ had fine and equiaxed grains due to the recrystallization, while nano-sized alumina particles distributions were different because they received a different stirring action.

In the case of FSW of Al alloy (Ref 14), grain structures in the TMAZ and the SZ were quite different. The TMAZ and SZ of FSW of Al alloy represented dynamic recovery and recrystallized structure, respectively, because high stacking fault energy of Al alloy resulted in the retaining of recovered structure in TMAZ. Mg alloys having hexagonal close packed (HCP) structure can be more easily recrystallized even at the TMAZ, consequently, FSW of Mg alloy resulted in the same recrystallized grain structure in the TMAZ and SZ (Ref 15).

The grain size of the AZ91 matrix was obviously refined by the FSP as shown in Fig. 5. It seems that the grain refinement was caused due to dynamic recrystallization during the FSP (Ref 13). However, the FSP with the nano-sized Al_2O_3 particles more effectively reduced the grain size of the AZ91 as-cast matrix in comparison with micron size particles in which some grains were less than 3 μm as shown in Fig. 5(b-d). It is considered that the pinning effect by the Al_2O_3 particles restricted the grain growth of the AZ91 matrix. The fine grain is very useful for enhancing the mechanical properties. Quantitative result of the average Al_2O_3 cluster size and the average AZ91 matrix grain size for surface composite layers produced by various FSP tools and particle sizes are listed in Table 2. The resulting grain size is significantly refined from the initial grain size of ~150 μm for the AZ91 as-cast. Assuming a completely uniform distribution of clustering nano-sized Al_2O_3 particles, the Zener limiting grain size (dz) can be calculated by the equation $dz = 4r/3Vf$, where r and Vf are the radius and volume fraction of clustering Al_2O_3 particles, respectively (Ref 13).

The measured AZ91 matrix grain size can be related to the Zener limiting grain size. This suggests that the presence of finely dispersed Al_2O_3 particles can limit the grain growth and result in an ultrafine grain size in the AZ91 matrix. If all of the Al_2O_3 particles are separated, and are completely and uniformly dispersed, the theoretically estimated grain size may be decreased specially in nano-size particles. It is the key point that the alumina particles must be finely dispersed. Hence, if one can completely disperse the nano-alumina particles in the

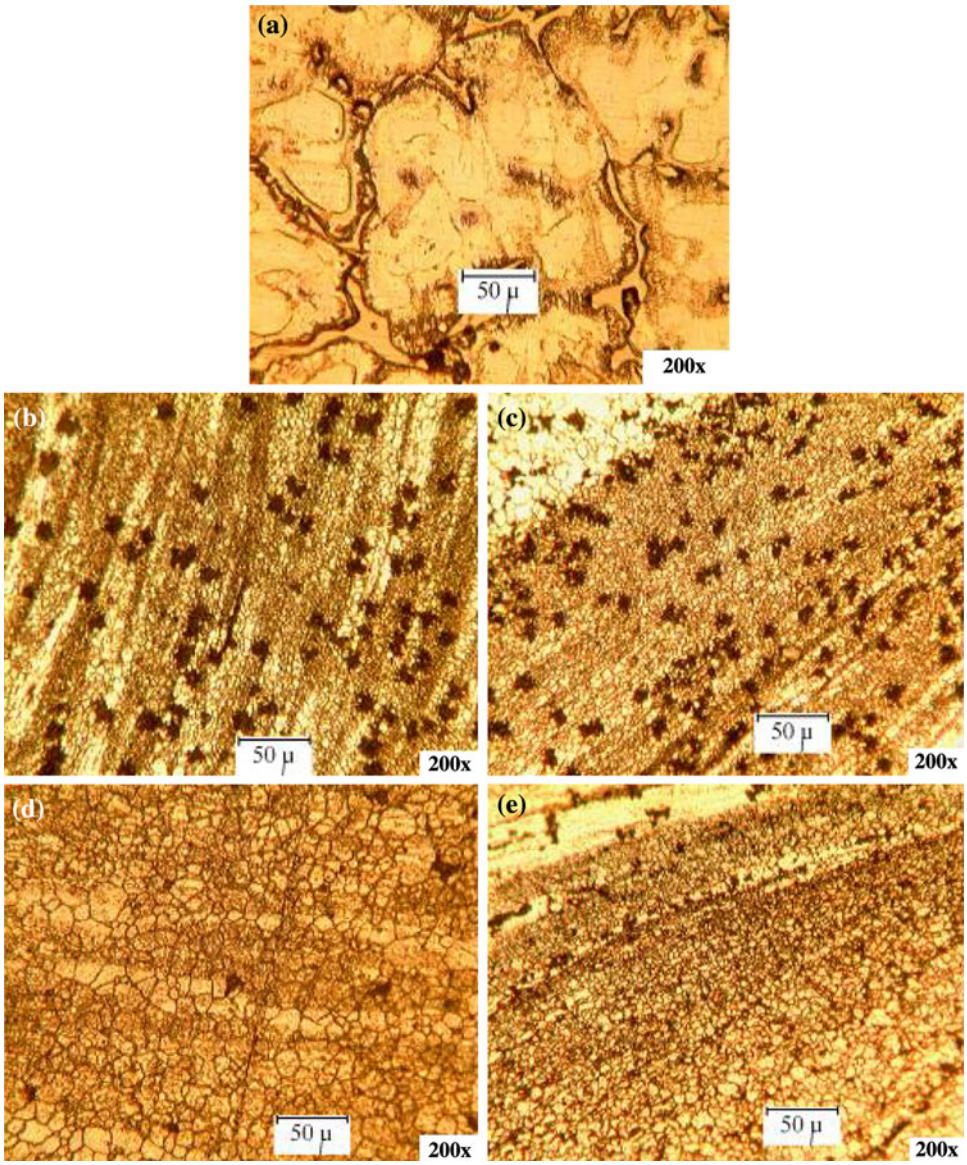

Fig. 5 Effect of alumina particle size and tool geometry on grain size and cluster size (a) base metal, (b, c, and d) FSPed specimen with 0.03, 0.3, 3 μm alumina particle size by square tool, respectively, (e) FSPed specimen with 0.3 μm alumina particle size by triangular tool

FSPed zone, it could produce the nano-grain-sized composite. It seems that increasing the number of passes could be the best choice to disperse the alumina particles uniformly. It follows that a certain level of local clustering is inevitable, and not all nano-particles can restrict grain boundary migration. The microstructures in the FSPed specimens with nano-fillers can be refined to a much smaller scale than the FSPed parent alloy without alumina particles. Figure 5 shows the effect of alumina particle size and tool geometry on grain size and cluster size of surface composite. A representative microstructure and grain size of the BM is shown in Fig. 5(a), which is shown the lighted α-phase embedded by dark β-phase ($Mg_{17}Al_{12}$) in the grain boundary. It can be seen that the grain size of the BM is about 130 μm. Figure 5(b-d) shows FSPed specimens with 30, 300, and 3000 nm alumina particle size by square tool, respectively, and Fig. 5(e) shows the FSPed specimen with 300 nm alumina particle size by triangular tool. From this figure, one can see that the triangular tool geometry is better than square tool because of better grain refinement and good particle dispersion. This result is in good agreement with (Ref 16). The reason might be attributed to better vigorous stirring during the FSP with triangular tool in comparison with square tool due to shape and sharp corners of the triangle tool (Ref 16).

Grain refinement in the case of composite samples may be attributed to the presence of reasonably uniformly distributed Al_2O_3 particulates which act as nuclei and also restricted grain growth during solidification. Furthermore, grain refinement of matrix due to secondary processing can be attributed to the coupled effects of (i) capability of Al_2O_3 particulates to nucleate magnesium grains during recrystallization and (ii) restricted growth of recrystallized magnesium grains as a result of presence of Al_2O_3 particulates. The fundamental principles behind the ability of inclusions in the metallic matrix to nucleate recrystallized grains and to inhibit grain growth have been already established (Ref 1) and will not be discussed here.

Dispersion of the nano-reinforcements in a uniform manner is a critical and difficult task (Ref 13). Figure 6 shows the effect of pass number on microstructure, grain size and cluster size of the specimen produced by square and triangular tool in which the rotational and traverse speed was 900 rpm and 63 mm/min. From Fig. 6, it can be seen that the grain size and cluster size in the specimen produced by the triangular tool is smaller than that of square tool. Also, increasing of the pass number in FSP is the effective method to produce homogenized and ultra fine-grain microstructure. Table 2 shows the quantitative data of grain size and cluster size.

Table 2 Effect of the number of passes and tool geometry on grain size, cluster size and Zener limiting size

	Average grain size, μm		Average cluster size, μm		Zener limiting size, μm	
Number of passes	Triangular tool	Square tool	Triangular tool	Square tool	Triangular tool	Square tool
Single pass	5.63	6.7	3.8	9.3	25.3	62
Three passes	2.16	2.8	1.7	2.5	11.3	16.6

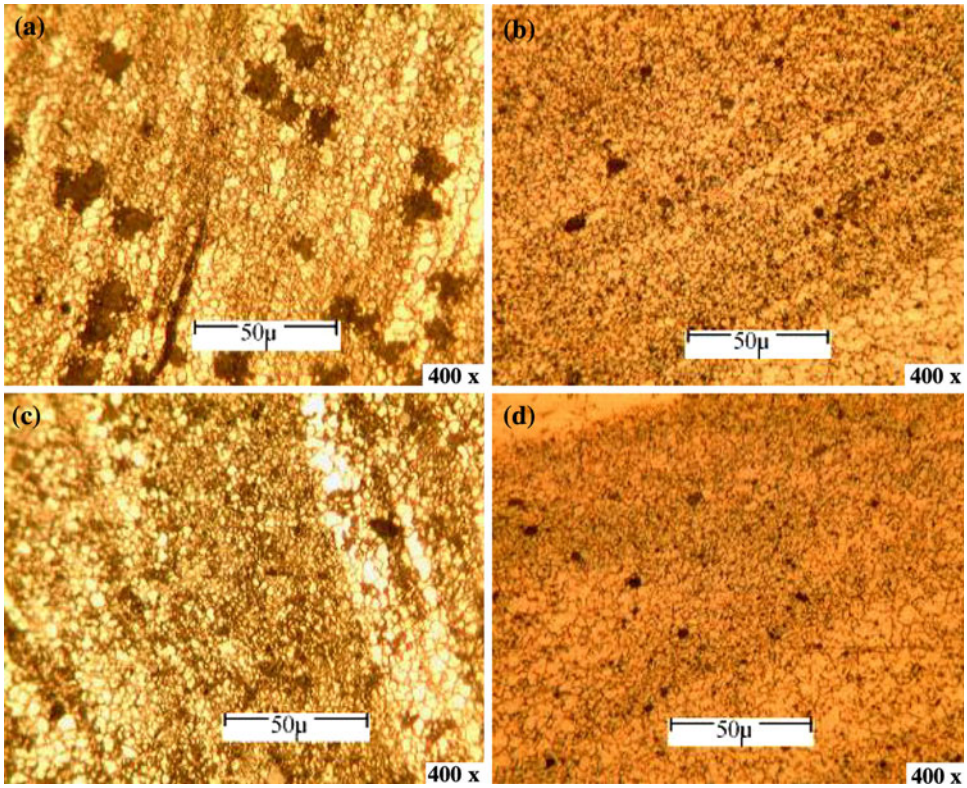

Fig. 6 Optical micrograph of the specimens produced in rotational and traverse speed 900 rpm and 63 mm/min, in which the particle size was 0.3 μm, (a) square tool, single pass, (b) square tool, three pass, (c) triangular tool, single pass, and (d) triangular tool, three pass

Table 3 Average micro-hardness and grain size of the surface at the stir zone of specimens

Material	Average micro-hardness, Hv		Average grain size, μm	
	FSP with alumina particles	FSP without particles	FSP with alumina particles	FSP without particles
AZ91 as-cast	70	70	~150	···
AZ91 FSP/square tool/particle size 3000 nm	98	97.11	9.63	···
AZ91 FSP/square tool/particle size 300 nm	101.3	96.87	6.7	···
AZ91 FSP/square tool/particle size 30 nm	103.2	98.52	5.94	7.27
AZ91 FSP/triangular tool/particle size 300 nm	102.9	97.33	5.63	···

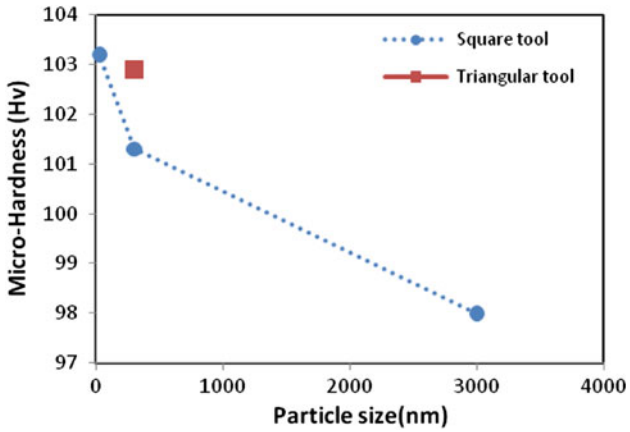

Fig. 7 Effect of particle size and tool geometry on micro-hardness

3.2 Micro-hardness Study

The effect of Al_2O_3 particle size on the resulting hardness is shown in Table 3 and Fig. 7 where it is observed that decreasing the particle size leads to increase in the hardness. At least five separate measurements were performed at the SZ of each sample. The average values of these five measurements were tabulated in Table 3.

From Fig. 7, one can see that the triangular tool can produce finer grain size rather than the square tool. This is because of the finer particle size can produce finer grain size and higher micro-hardness. This result is expected since the grain size reached during processing decreases as a result of smaller particle size used.

Figure 8 shows the micro-hardness profile of the specimen number 2 in the AB direction shown in Fig. 8(a). From this figure, the micro-hardness of the region near the upper surface is higher than that in the region far from upper surface.

Figure 9 shows the effect of tool geometry and the number of passes on micro-hardness profile of the specimen sections. From the figure, harder surface composite can be produced by triangular tool geometry in high number of FSP passes. On the other word, hardness of the specimen produced by triangular tool is higher than that of square tool. The figure shows that surface hardness of the sample increases with the number of passes. Increasing the number of passes cause to produce a surface composite with better homogeneity and good distribution of the particulates and smaller grain size.

According to Ref 17, the coarse eutectic β-$Mg_{17}Al_{12}$ network in the as-received AZ91 was disappeared after FSP, because the temperature of the SZ exceeded the dissolution

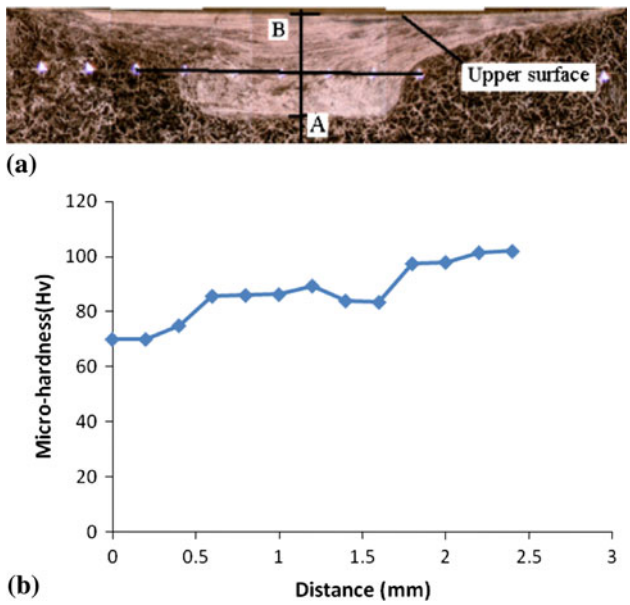

Fig. 8 (a) AB direction and (b) micro-hardness profile of the specimen 2

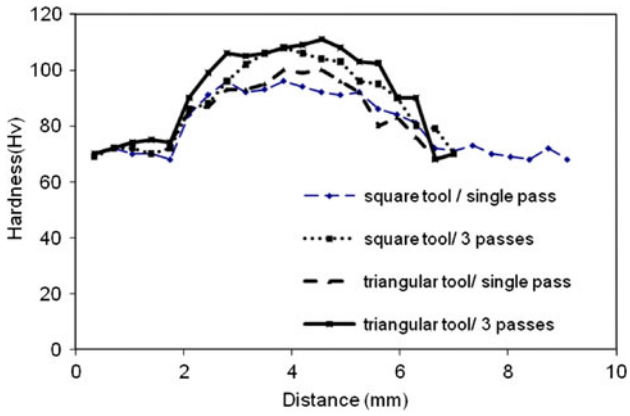

Fig. 9 Effect of tool geometry and number of passes on micro-hardness profile

temperature of the β-phase in the Mg matrix. The refinement of grain size are mainly affected by the parameters of the FSP, such as traverse speed, rotation speed, etc., and slightly affected by the addition of Al_2O_3. It seems that the grain refinement was caused due to dynamic recrystallization during the FSP

(Ref 15). The FSP with the Al_2O_3 particles is considered to make finer grains due to enhancement of the induced strain and the pinning effect by the Al_2O_3 particles. Agglomerated nano-sized alumina particles have not good distribution in the field. The observed clustering particle is frequently 0.1-0.2 μm in the SZ, much larger than the individual Al_2O_3 size (30 nm). Though, the dispersion of nano-Al_2O_3 particles is not uniform, the grain size on the nano-sized Al_2O_3 particles/AZ91 stir region (~5.94 μm) is slightly smaller than that of AZ91 (~7.27 μm) SZ under similar condition (see Table 3). Moreover, the micro-hardness of the nano-sized Al_2O_3 particles/AZ91 SZ (~103 Hv) is slightly greater than that of the AZ91 (~98 Hv) SZ under the same FSP condition (see Table 3). Presence of agglomerated nano-sized alumina particles and not uniform distribution of nano-sized alumina particles cause to slightly affect the hardness of the SZ.

The as-received AZ91 was characterized by a coarse eutectic β-$Mg_{17}Al_{12}$. The magnesium matrix in the as-received AZ91 casting contains 9 wt.% Al. This value is higher than the room-temperature equilibrium concentration of aluminum in magnesium, indicating that the as-received AZ91 is a little supersaturated. Based on the Mg-Al phase diagram, a heating temperature of 437 °C causes the dissolution of the eutectic β-$Mg_{17}Al_{12}$ phase into the magnesium matrix. For Mg-Al alloys, it takes up to ~40 h to achieve the complete dissolution of the eutectic β-$Mg_{17}Al_{12}$ phase due to low diffusion rate of aluminum in magnesium matrix (Ref 18). For the FSW/FSP thermal cycles, both heating and cooling rates are quite high. For example, the duration at above 200 °C during FSP of A356 aluminum alloy is only 25 s (Ref 19). It seems impossible to achieve the dissolution of most of the eutectic β-$Mg_{17}Al_{12}$ phase in such a short period for a conventional thermal cycle. However, for FSW/FSP, severe plastic deformation in the SZ, with a strain rate of 10^0-10^2 s^{-1} and a strain of up to 0.4% (Ref 20, 21), facilitates significantly the dissolution of the β-$Mg_{17}Al_{12}$ phase, thereby generating an aluminum-supersaturated solid solution. The uniform distribution of reinforcement in the case of composites can be attributed to (a) good wetting of reinforcement by the matrix (Ref 15) and (b) dynamic stirring action.

3.3 X-ray Diffraction

Figure 10 shows XRD analysis for the FSPed AZ91 sample and initial as-cast AZ91 alloy. From the figure, original pick width in comparison with the FSPed specimens satisfies the grain refinement after processing. A shift of the picks for the FSP sample satisfies large deformation in crystallographic planes. It was suggested that it is possible to measure the grain size using XRD analysis by using Scherrer Formula (Ref 22)

$$D = \frac{k \times \lambda}{\beta \times \cos\theta} + \eta \tan\theta, \qquad \text{(Eq 1)}$$

where D is the grain diameter, β is the peak width in radians at full width at half maximum (FWHM) after correction for instrumental broadening, k is Scherrer constant estimated about 0.9-1, and η is the strain in the material. According to the Eq 1, the grain sizes of FSPed AZ91 sample and as-cast AZ91 sample are estimated as ~8 and ~134 μm, respectively, which are very close to those obtained in Fig. 5. In this study, the micro-strain term was assumed to be zero.

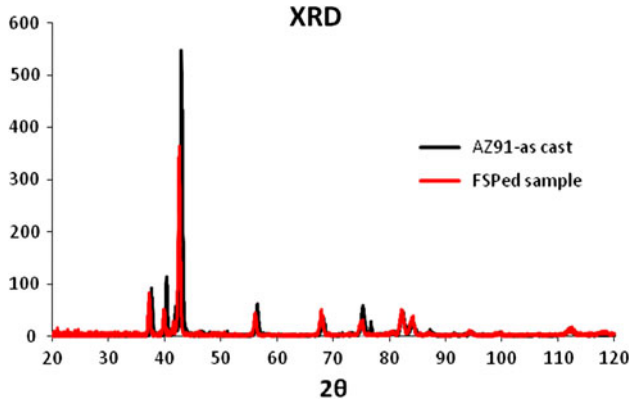

Fig. 10 XRD studies for the as-cast AZ91 and FSPed sample with square tool and particle size of 300 nm

4. Conclusion

Al_2O_3 particles can be used as reinforcement and grain refinement. The microstructures in the FSPed specimens with nano-Al_2O_3 particles can be refined to a much smaller scale than the FSPed parent alloy without alumina particles. The recrystallized grains were equiaxed and have a similar size distribution. Al_2O_3 particles were found to be distributed within this region due to the occurrence of vigorous stirring during the process. Grain structures in the SZ had fine and equiaxed grains due to the recrystallization, while nano-sized alumina particles distributions were different because they received a different stirring action. It was shown that the grain size and cluster size in the specimen produced by the triangular tool is smaller than that of square tool. Also, increasing of the pass number in FSP is the effective method to produce homogenized and ultra fine-grain microstructure. The results show that decreasing the particle size leads to increase in the hardness. Hardness of the specimen produced by triangular tool is higher than that of square tool and increasing the number of passes leads to monotonous hardness curve.

References

1. S.F. Hassan and M. Gupta, Effect of Particulate Size of Al_2O_3 Reinforcement on Microstructure and Mechanical Behavior of Solidification Processed Elemental Mg, *J. Alloys Compd.*, 2006, **419**, p 84–90
2. Y. Morisada, H. Fujii, T. Nagaoka, and M. Fukusumi, Effect of Friction Stir Processing With SiC Particles on Microstructure and Hardness of AZ31, *Mater. Sci. Eng. A*, 2006, **433**, p 50–54
3. Y. Morisada, H. Fujii, T. Nagaoka, and M. Fukusumi, MWCNTs/AZ31 Surface Composites Fabricated by Friction Stir Processing, *Mater. Sci. Eng. A*, 2006, **419**, p 344–348
4. C.I. Chang, Y.N. Wang, H.R. Pei, C.J. Lee, X.H. Du, and J.C. Huang, Microstructure and Mechanical Properties of Nano-ZrO_2 and Nano-SiO_2 Particulate Reinforced AZ31-Mg Based Composites Fabricated by Friction Stir Processing, *Key Eng. Mater. Compos. Mater. V*, 2007, **351**, p 114–119
5. C.I. Chang, Y.N. Wang, H.R. Pei, C.J. Lee, and J.C. Huang, On the Hardening of Friction Stir Processed Mg-AZ31 Based Composites with 5-20% Nano-ZrO_2 and Nano-SiO_2 Particles, *Mater. Trans.*, 2006, **47**, p 2942–2949
6. B.M. Darras, M.K. Khraisheh, F.K. Abu-Farha, and M.A. Omar, Friction Stir Processing of Commercial AZ31 Magnesium Alloy, *J. Mater. Process. Technol.*, 2007, **191**, p 77–81
7. R. Gunther, Ch. Hartig, and R. Bormann, Grain Refinement of AZ31 by $(SiC)_p$: Theoretical Calculation and Experiment, *Acta Mater.*, 2006, **54**, p 5591–5597

8. A.A. Kaya, E.S. Kayak, D. Eliezer, G. Gertsberg, and N. Moscovitch, Addition of B_4C to AZ91 via Diecasting and its Effect on Wear Behavior, *Proceedings of the International Conference on Magnesium—Science, Technology and Applications*, Materials Science Forum, 2005, p 741–744
9. A. Kleine, J. Hemptenmacher, H.J. Dudek, K.U. Kainer, and G. Krueger, Interface Formation in Carbon Fiber Reinforced Magnesium Alloys (AZ91), *J. Mater. Sci. Lett.*, 1995, **14**, p 358–360
10. G. Vidrich, O. Moll, and H. Ferkel, Grain Refinement of Mg Alloys by Nanoscaled TiN Particles, *J. Mater.*, 2004, **56**, p 84
11. K. Xiu, H.Y. Wang, H.L. Sui, Y. Wang, C.L. Xu, J.G. Wang, and Q.C. Jiang, The Sliding Wear Behavior of TiC_p/AZ91 Magnesium Matrix Composites, *J. Mater. Sci.*, 2006, **41**, p 7052–7058
12. A.J. Ardell, Precipitation Hardening, *Metall. Mater. Trans. A*, 1985, **16**, p 2131–2165
13. A.S. Zarghani, S.F.K. Bozorg, and A.Z. Hanzaki, Microstructures and Mechanical Properties of Al/Al_2O_3 Surface Nano-Composite Layer Produced by Friction Stir Processing, *Mater. Sci. Eng. A*, 2008. doi: 10.1016/j.msea.2008.09.064
14. J.Q. Su, T.W. Nelson, R. Mishra, and M. Mahoney, Microstructural Investigation of Friction Stir Welded 7050-T651 Aluminum, *Acta Mater.*, 2003, **51**, p 713–729
15. W.B. Lee, C.Y. Lee, M.K. Kim, J.I. Yoon, Y.J. Kim, Y.M. Yoen, and S.B. Jung, Microstructures and Wear Property of Friction Stir Welded AZ91Mg/SiC Particle Reinforced Composite, *Compos. Sci. Technol.*, 2006, **66**, p 1513–1520
16. G. Padmanaban and V. Balasubramanian, Selection of FSW Tool Pin Profile, Shoulder Diameter and Material for Joining AZ31B Magnesium Alloy—An Experimental Approach, *Mater. Des.*, 2009, **30**, p 2647–2656
17. A.H. Feng and Z.A. Ma, Enhanced Mechanical Properties of Mg-Al-Zn Cast Alloy Via Friction Stir Processing, *Scr. Mater.*, 2007, **56**, p 397–400
18. S. Kleiner, O. Beffort, and P.J. Uggowitzer, Microstructure Evolution During Reheating of an Extruded Mg-Al-Zn Alloy into the Semisolid State, *Scr. Mater.*, 2004, **51**, p 405–410
19. Z.Y. Ma, S.R. Sharma, and R.S. Mishra, Microstructural Modification of As-Cast Al-Si-Mg Alloy by Friction Stir Processing, *Metall. Mater. Trans. A*, 2006, **37A**, p 3323–3336
20. P. Heurtier, C. Desrayaud, and F. Montheillet, A Thermomechanical Analysis of the Friction Stir Welding Process, *Mater. Sci. Forum*, 2002, **396–402**, p 1537–1542
21. C.I. Chang, C.J. Lee, and C. Huang, Relationship Between Grain Size and Zener-Holloman Parameter During Friction Stir Processing in AZ31Mg Alloys, *Scr. Mater.*, 2004, **51**, p 509–514
22. B.D. Cullity, *X-Ray Diffraction*, 3rd ed., Prentice-Hall, Upper Saddle River, 2001